Catal Lett (2017) 147:62–70
DOI 10.1007/s10562-016-1881-8

Effect of Steam During Fischer–Tropsch Synthesis Using Biomass-Derived Syngas

Zi Wang[1] · Khiet Mai[1] · Nitin Kumar[1] · Thomas Elder[2] · Leslie H. Groom[2] · James J. Spivey[1]

Received: 16 June 2016 / Accepted: 29 September 2016 / Published online: 17 November 2016

Abstract Fischer–Tropsch synthesis (FTS) with biomass-derived syngas was performed using both iron-based 100Fe/6Cu/4K/25Al catalyst and ruthenium-based 5 % Ru/SiO_2 catalyst. During FTS, different concentrations of steam were co-fed with the biomass-derived syngas to promote the water gas shift reaction and increase the H_2/CO ratio. On Fe-based catalysts the increase in steam concentration led to lower conversion, while deactivation is not observed on Ru-based catalysts. XRD of the spent iron-based catalyst showed the oxidation of iron carbides. Adding steam inhibited surface carbon deposition, as measured by temperature programmed hydrogenation. The iron carbide phase could be re-carburized by flowing CO. The addition of steam had different effects on these two catalysts. Fe-based catalyst showed significantly lower methane selectivity and greater C_{5+} hydrocarbon selectivity, while on the Ru-based catalyst, adding steam only showed slightly decreased methane selectivity.

Graphical Abstract

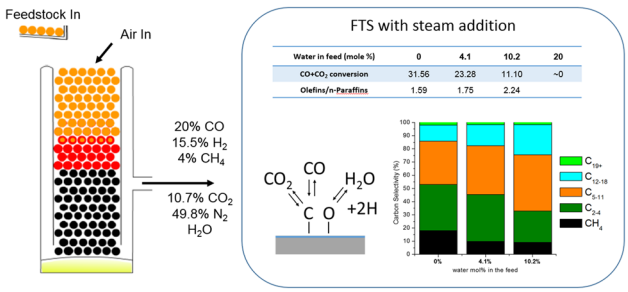

1 Introduction

The gasification of biomass is a promising technique to generate different forms of valuable alternative energy, including direct thermal energy and further conversion of synthesis gas to clean liquid fuels or chemicals via Fischer–Tropsch synthesis (FTS) [1–5]. The ideal H_2/CO ratio for FTS is ~2/1 based on the stoichiometry. However, The H_2/CO for the synthesis gas obtained from biomass gasification is considerably lower, typically ~0.7/1. Elder et al. [6] studied the gasification of biomass using an air-blown pilot-scale gasification system at various conditions. Based on a ~17–30 kg h^{-1} wood chips feedstock, the unit produce 855 dm^3 m^{-3} gas with the composition of 20 % carbon monoxide, 15.5 % hydrogen, 4 % methane, 10.7 % carbon dioxide and balance nitrogen [6], which is representative of syngas produced in these types of biomass gasifiers [7, 8]. This hydrogen-deficient type of syngas requires Fe and Ru-based FTS catalyst to promote the water-gas-shift reaction.

During FTS, the steam formed can react with CO to produce CO_2 and hydrogen via the water gas shift reaction ($H_2O + CO \rightarrow H_2 + CO_2$), producing the required hydrogen

✉ James J. Spivey
jjspivey@lsu.edu

[1] Department of Chemical Engineering, Louisiana State University, S. Stadium Drive, Baton Rouge, LA 70803, USA

[2] USDA Forest Service, Southern Research Station, Pineville, LA 71360, USA

needed for FTS [9]. Depending on the specific gasifier, the gasification of biomass can produce significant levels of steam, yet there are relatively few studies on the systematic effect of adding steam to the biomass-derived syngas, despite the potential positive effect of added steam. Satterfield et al. [10] reported that steam added to dry synthesis gas increased the water–gas shift rate, as expected. Steam addition also reduced methane selectivity and increased oxygenate selectivity. In terms of conversion, the steam with 27 mol% in the feed decreased the catalyst activity, while the activity could be recovered once the steam was removed. However, 42 mol% steam in the feed caused irreversible deactivation. Pendyala et al. [11] studied the effect of steam on a potassium-promoted precipitated Fe-based catalyst during FTS at 230 and 270 °C. At lower temperature (230 °C) the addition of steam decreased FTS activity and oxidized the Fe carbide. However, no signs of oxidization were found when steam was added to the feed at 270 °C.

Ruthenium-based catalysts have also been used to study the effect of added steam. Claeys et al. [12] investigated the effect of steam during FTS over a ruthenium supported on SiO_2 catalyst. The addition of water led to lower methane selectivity and enhanced chain growth probability. CO conversion also increased upon steam addition. They claim that steam served as a moderator during FTS, minimizing carbon deposition and supplying a source of hydrogen for the formation of hydrocarbon monomers.

Although the addition of steam in FTS has been studied on various catalysts using fixed-bed reactors or slurry stirred reactors [13–16], the synthesis gases used in their reports usually contain only CO and H_2 with the H_2/CO ratio ranging from 1/1 to 2/1. To our knowledge, we are not aware of systematic reports on the effect of added steam in FTS using biomass-derived syngas, especially at low H_2/CO ratios and high inert N_2 concentration.

In the present study, we report the effect of adding 4–20 mol% steam on the CO conversion and product selectivity of two types of catalysts: (1) A Fe-based catalyst with potassium and copper as promoters to suppress methane formation, and aluminum oxide as structural promoters to prevent catalyst oxidation. (2) An unpromoted Ru/SiO_2 as a comparison based on the effect of added steam in decreasing methane selectivity and increasing chain growth probability over Ru-based catalysts [12].

2 Experimental

The iron-based catalyst was synthesized by coprecipitation. Iron(III) nitrate [$Fe(NO_3)_3{\cdot}9H_2O$, Sigma-Aldrich], copper(II) nitrate [$Cu(NO_3)_3{\cdot}2.5H_2O$, Sigma-Aldrich] and aluminum nitrite [$Al(NO_3)_3{\cdot}9H_2O$, Alfa Aesar] were first mixed and dissolved in deionized water. Then the aqueous solution was titrated into a continuous-stirred beaker with 100 ml water at 80 °C, while 1 M $(NH_4)_2CO_3$ solution was added dropwise to maintain the pH at 7.00 ± 0.2. The brown-colored precipitate solution was aged for 4 h, afterwards the precipitate was collected by filtration and the solid was washed with ethanol. The precipitate was kept in the oven at 120 °C for 24 h. A desired amount of $KHCO_3$ solution was impregnated into the catalyst precursor using the incipient wetness impregnation method. After the impregnation, the catalyst was calcined at 360 °C for 6 h under 50 ml/min nitrogen flow. Based on the ICP-OES analysis, the catalyst has the atomic ratio of 100Fe/6Cu/4K/25Al. The catalyst is labeled as Fe/Cu/K/Al.

The ruthenium supported on SiO_2 catalyst was prepared by impregnating ruthenium nitrosylnitrate (Alfa Aesar) solution onto SiO_2 (PQ Corporation). The impregnated precursor was dried at 110 °C for 24 h, followed by the calcination at 300 °C for 4 h under nitrogen flow. The final catalyst has 5 wt% of Ru. This catalyst is denoted as Ru/SiO_2.

Scanning electron microscopy (SEM) and energy-dispersive X-ray spectroscopy (EDX) were carried out on a Quanta 3D DualBeam FEG FIB-SEM to study the morphology and surface element composition changes of the used Fe/Cu/K/Al catalyst after FTS with steam addition. The accelerating voltage is set at 20 kV, and the energy-dispersive spectra (EDS) of the samples are generated from the SEM images at ×1000 magnification.

An Empyrean X-ray diffractometer with Cu Kα radiation ($\lambda = 0.15406$ nm) was used for XRD analysis on fresh and used Fe/Cu/K/Al catalyst. The XRD patterns were collected from 15° to 90° for Fe-based catalyst. The patterns were analyzed using the X'pert HighScore Plus software with the Search & Match feature.

Fischer–Tropsch synthesis was performed on a PID EFFI microactivity reactor. The biomass-derived syngas used in the reaction has the composition of 20% carbon monoxide, 15.5% hydrogen, 4% methane, 10.7% carbon dioxide and balance nitrogen. The iron-based catalyst requires a carburization step prior to the reaction. During each run, 1 g of catalyst was mixed with 5 g of sand, and loaded into a 1 inch stainless steel reactor. The reactor was first heated to 280 °C under helium flow, then 30 sccm of carbon monoxide flowed through the reactor for 24 h to reduce and carburize the catalyst at 280 °C and 1 bar. Ru/SiO_2 was reduced in H_2/He prior to the reaction. 2.5 g of catalyst was loaded into the reactor. 5 sccm of H_2 and 25 sccm of He flowed through the reactor, and the temperature is ramped to 300 °C. The catalyst is reduced at this temperature in hydrogen for 4 h.

The reaction was carried out at 270 °C on both the carburized Fe-based catalyst and the reduced Ru-based

catalyst. After the pretreatment step, the temperature is lowered to 270 °C, and 40 sccm of biomass-derived syngas and 7 sccm helium was mixed and flowed through the reactor. The reactor pressure is set at 20 bar. The reaction was kept at this condition for 120 h, and the liquid products (hydrocarbons and alcohols) were collected in the liquid traps. Then different amounts of steam were injected into the feed. A certain amount of water was pumped by a Gilson 307 pump into the vaporizer, which was kept at 180 °C to vaporize the steam. Steam is subsequently mixed with the syngas-helium flow and injected into the reactor. Helium inert flow was adjusted when steam was injected to keep the space velocity constant. The composition of steam was 4.1, 10.2 % and 20.5 mol% of the total flow. Liquid products were collected at the end of each run. Liquid hydrocarbon and oxygenate analysis were conducted by GC-FID from Emerging Fuel Technology (EFT) in Broken Arrow, OK.

Temperature programmed hydrogenation (TPH) is tested on Fe/Cu/K/Al to examine the carbonaceous species on the surface and in the bulk of the catalysts. In each test, 100 mg catalyst was initially pretreated with 50 sccm of 5 % CO/He at 280 °C for 16 h, followed by the CO hydrogenation reaction at different conditions, including: (1) 10 h reaction at 270 °C and 1 atm with simulated biomass-derived syngas (20 % CO, 15.5 % H_2, 4 % CO_2 and balance He); (2) 10 h reaction at 270 °C and 1 atm with the simulated biomass-derived syngas, but flowed through a saturator filled with water prior to the reactor; (3) the same reaction conditions as (2), followed by a regeneration step with 5 % CO/He at 280 °C for 16 h. After the treatments, TPH pattern was collected by flowing 15 sccm H_2 through the reactor, and the temperature was ramped to 950 °C at 5 °C/min.

3 Results and Discussion

FTS over the Fe/Cu/K/Al catalyst and Ru/SiO_2 catalyst were carried out with different concentrations of added steam in the syngas. Table 1 shows the CO and CO_2 conversions and the hydrocarbon distribution of Fe/Cu/K/Al. [No significant activity was observed for the run with 20 % steam, thus, the conversion and production distribution for Fe/Cu/K/Al at 20 % steam addition level is not presented in Table 1.]

FTS on Fe/Cu/K/Al with 0 % steam addition has a total conversion ($CO+CO_2$) of 31.6 %, which is similar to the conversion reported in previous studies of using biomass-derived syngas for FTS [17–19]. The addition of steam in the feed caused decreased CO conversion, and the reaction is completely quenched with 20 % steam co-feeding. The rate equations for the iron-based FTS catalyst in a fixed bed reactor can be expressed as [20, 21]

Table 1 $CO+CO_2$ Conversion, hydrocarbon distribution and olefin/paraffin ratio of Fe/Cu/K/Al at 270 °C, 20 bar, GHSV = 2820 scc $gcat^{-1}$ h^{-1}

Steam in feed (mol%)	0	4.1	10.2
$CO+CO_2$ conversion (%)	31.6	23.3	11.1
CO conversion (%)	26.6	23.3	21.6
CO_2 conversion (%)	40.1	23.2	−6.9
HC selectivity (C%)			
CH_4	15.5	8.1	7.4
C_2–C_4	30.0	29.7	19.2
C_5–C_{11}	28.2	30.7	34.5
C_{12}–C_{18}	10.4	13.3	18.6
C_{19+}	1.8	1.4	1.4
Olefins/n-Paraffins			
$C_5^=$–$C_{11}^=$/n–C_5–C_{11}	1.6	1.8	2.2
$C_{12}^=$–$C_{18}^=$/n–C_{12}–C_{18}	0.7	0.8	0.9

The compositions are calculated based on a 24 h accumulative run at the steady state

$$r_{FT} = A\frac{P_{H_2}P_{CO}}{P_{CO} + k_{H_2O}P_{H_2O}} \quad (1)$$

Therefore, steam co-feeding would expect to inhibit the rate for FTS. Table 1 shows that the presence of steam inhibits $CO+CO_2$ conversion, which is consistent with the rate expression (Eq. 1), This is caused by (1) the decrease of CO partial pressure due to higher WGS rate [22], and (2) the oxidation of the catalyst, as detected by XRD, SEM and TPH. The analysis of catalyst oxidation will be discussed later in this section.

The addition of steam increased the selectivity to higher hydrocarbons, especially for C_{5+} hydrocarbons on the Fe/Cu/K/Al catalyst. The selectivity to C_5–C_{11} increased from 28.2 to 34.5 % at 10.2 % steam in the feed, and the C_{12}–C_{18} selectivity increased from 10.4 to 18.6 %. The effect of added steam agrees with the results obtained on cobalt-based FTS catalysts [23–27]. The increased composition of H_2 facilitates the hydrogenation of dissociated or undissociated CO, which is a rate limiting step in the conversion of CO to hydrocarbons [21, 28, 29]. Therefore, the increase of H_2/CO ratio leads to higher hydrocarbon selectivity. In addition, Schultz et al. [27] state that adding steam inhibits the desorption of monomers and short-chain products, thus, the chain growth rate increases to favor the formation of higher hydrocarbons. Olefins to n-paraffins ratio also increases due to the added steam. For C_5–C_{11} hydrocarbons the ratio of olefins/paraffins increased from 1.59 to 2.24 at 10.2 % steam addition. Satterfield et al. [10] reported considerably decrease in methane selectivity with steam addition during FTS reactions at 250 °C, consistent with the results here (Table 1). As mentioned above, the desorption

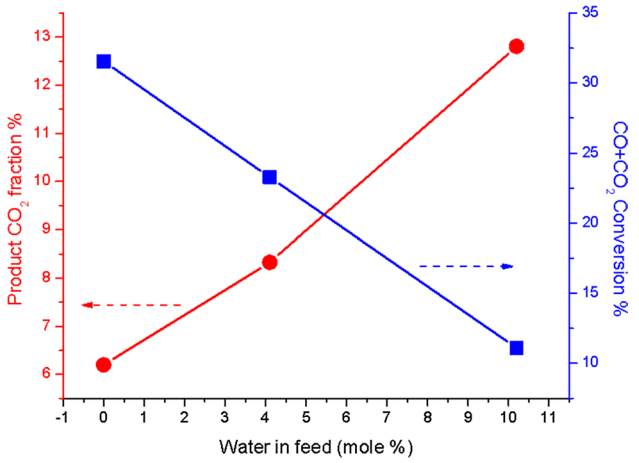

Fig. 1 CO_2 fraction in the product gas and FTS $CO+CO_2$ total conversion with steam in the feed. *Red line* production CO_2 fraction, %. *Blue line* $CO+CO_2$ total conversion, %

Table 2 $CO+CO_2$ conversion, hydrocarbon distribution and olefin/paraffin ratio of Ru/SiO_2 at 270 °C, 20 bar, GHSV = 2820 scc $gcat^{-1}h^{-1}$

Steam in feed (mol%)	0	4.1	10.2	20.5
$CO+CO_2$ conversion	11.8	11.1	11.3	9.8
CO conversion	10.0	11.7	11.3	9.0
CO_2 conversion	14.9	13.9	13.4	10.6
HC selectivity (C%)				
CH_4	14.5	14.9	13.1	12.7
C_2–C_4	17.5	18.0	15.8	14.2
C_5–C_{11}	32.0	34.4	33.7	34.6
C_{12}–C_{18}	17.2	17.5	17.5	17.3
C_{19+}	1.6	1.8	1.9	1.8
Olefins/n-Paraffins				
$C_5^=$–$C_{11}^=$/n–C_5–C_{11}	2.1	2.1	1.9	2.2
$C_{12}^=$–$C_{18}^=$/n–C_{12}–C_{18}	0.3	0.4	0.3	0.4

The compositions are calculated based on a 24 h accumulative run at the steady state

of monomers and short-chain hydrocarbons on the surface could be inhibited with the presence of steam. Therefore, the product distribution shifts to favor long-chain hydrocarbons when steam was added to the feed, while the selectivity to short-chain products such as methane and C_2–C_4 hydrocarbons is reduced. The olefin/paraffin ratio for C_2–C_5 also increases when the steam fraction was increased from 0 to 30 mol%.

Figure 1 shows the outlet CO_2 composition as a function of the added steam. For FTS with high CO_2 concentrations, CO_2 can be consumed by the reverse water–gas shift reaction to form CO and H_2O, or directly converted to hydrocarbons or oxygenates [30–32]. A considerable amount of CO_2 is hydrogenated into hydrocarbons with 0% steam addition, in which case as the outlet CO_2 fraction decreased from 10.7 to 6.2%. The addition of steam in the feed increased CO_2 concentration in the product gas (12.8%), which is higher than the CO_2 fraction in the feed. This suggests that water–gas shift activity is enhanced when steam was added. The enhanced WGS rate lead to higher H_2/CO ratio, which increases the selectivity to higher hydrocarbons in the reaction.

The conversion and hydrocarbon distribution for the Ru/SiO_2 catalyst is less influenced by the presence of steam (Table 2). The $CO+CO_2$ conversion slightly decreases as steam mol% increased, but the catalyst is still active at 20 mol% steam addition, unlike the Fe-based catalyst. Methane selectivity also decreased slightly at higher steam addition levels, consistent with the results of Cleays et al. [12]. The increasing steam concentration has little influence to the hydrocarbon selectivity and olefins/paraffins ratio.

XRD on the fresh and used Fe/Cu/K/Al catalysts were carried out to study the cause of deactivation at higher steam addition level. The XRD patterns for the fresh-calcined catalyst and the carburized catalyst in Fig. 2 show that the coprecipitated Fe/Cu/K/Al catalyst is XRD amorphous, even after the calcination and carburization process. The spectra for the sample after FTS with no steam co-feeding is denoted as "Dry FTS" in Fig. 2. The diffraction peaks with high intensities correspond to SiO_2 (JCPDS 01-078-1252), due to the inert silica used to dilute the catalyst. However, the sample shows no significant crystalline peaks for iron phases. The amorphous iron phase in the catalyst is maintained after FTS for 120 h.

XRD patterns of the samples after FTS with different level of steam addition are designated as "X% steam" in Fig. 2, where X% stands for the mol% of the added steam. Fe_3O_4 phase (JCPDS card 01-075-1609) is detected for the spent steam co-feeding samples, indicating the oxidation of the catalyst after FTS with steam addition. A comparison of the XRD patterns with $2\theta = 34°$ to 38° on the used catalysts is presented in Fig. 3. The peak at 35.537° corresponds to Fe_3O_4 (103). The crystallite size calculation based on Sherrer equation follows a sequence of 20% steam >10% steam >4% steam > Dry FTS. Therefore, the catalyst was oxidized after FTS with steam addition, and the Fe_3O_4 crystallites are larger at higher steam co-feeding conditions.

The SEM images of the Fe/Cu/K/Al catalyst under different steam co-feeding concentrations are shown in Fig. 4. The freshly calcined catalyst is composed of irregular, assorted particles with the average size varying from 10 to 25 µm, as seen in Fig. 2a. Fischer–Tropsch reaction with 10% steam co-feeding has minor changes on the catalyst morphology. However, when 20% of steam was added in the feed, the catalyst agglomerated as the average diameter of the catalyst particle increased to ~40 µm. EDS analysis was performed to determine the change of surface

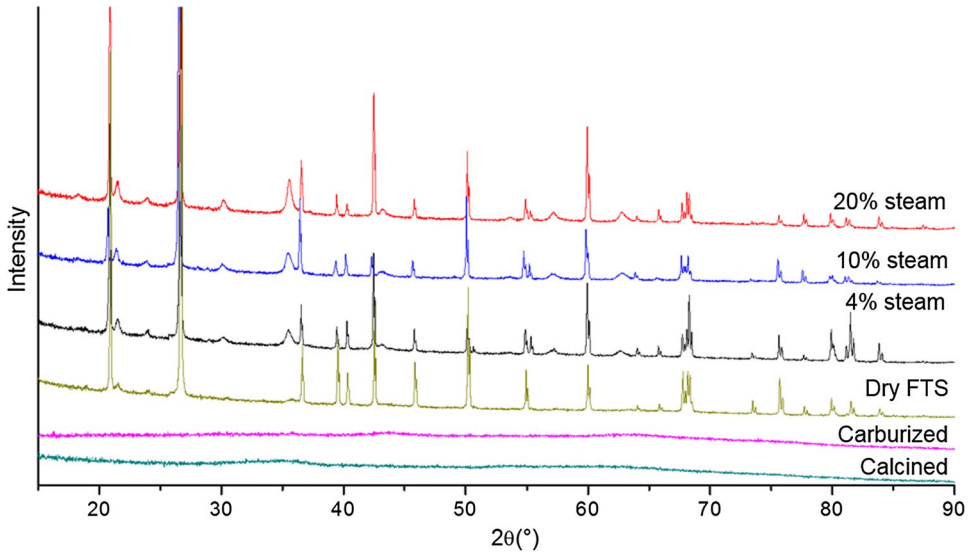

Fig. 2 X-ray diffraction spectra for the Fe/Cu/K/Al catalyst after (1) calcination, (2) carburization under CO, (3) FTS with no steam addition, (4) FTS with 4% steam, (5) FTS with 10% steam and (6) FTS with 20% steam addition

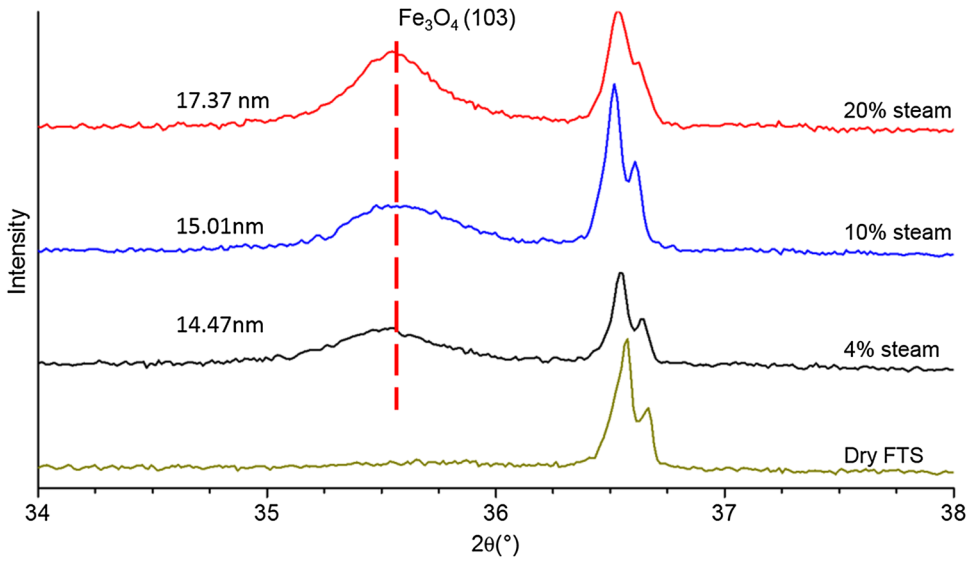

Fig. 3 X-ray diffraction spectra from 2θ = 34° to 38° for the Fe/Cu/K/Al catalyst after FTS under different levels of steam addition. The peak at 2θ = 35.537° corresponds to Fe_3O_4 (103) (JCPDS card 01-075-1609). The crystallite size is calculated by Scherrer equation

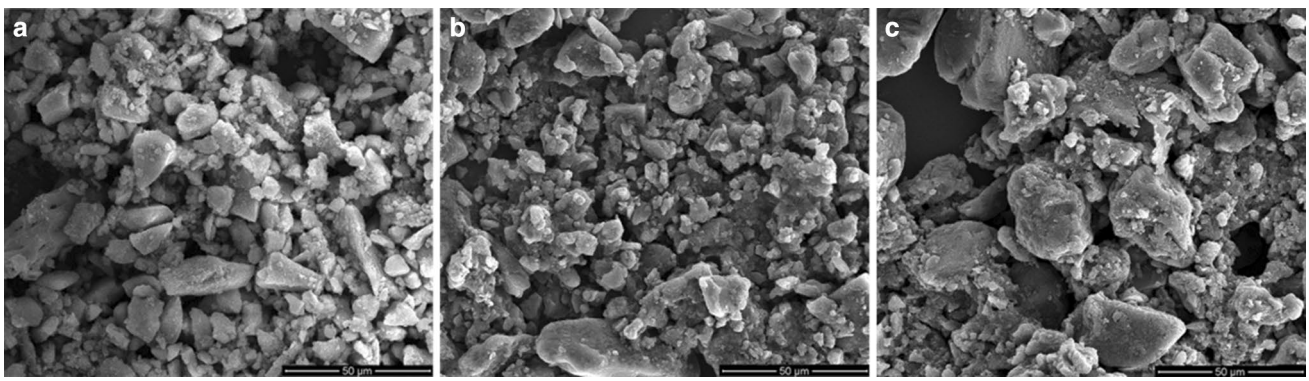

Fig. 4 SEM image at ×1000 of **a** calcined Fe/Cu/K/Al catalyst, **b** used Fe/Cu/K/Al catalyst after FTS with 10% steam co-feeding in syngas, **c** used Fe/Cu/K/Al catalyst after FTS with 20% steam co-feeding in syngas

composition after steam co-feeding. The atomic ratios of the major elements detected in the EDS are summarized in Table 3. The catalyst surface is dominated by carbon after carburization and dry FTS reaction. However, the surface carbon composition declined significantly when steam fraction increased from 10 to 20 %, and the atomic % of surface oxygen changed from 11 to 16 %. The results from XRD and SEM show that Fe/Cu/K/Al deactivates during steam co-feeding, which is due to the oxidation of Fe in the presence of H_2O and CO_2.

Table 3 Surface atomic composition of Fe/Cu/K/Al after calcination and FTS with steam co-feeding

Element[a]	Atomic %		
	Calcined	10 % steam	20 % steam
C	–	82.7	76.6
O	56.5	11.19	16.2
Al	6.6	0.9	1.1
Fe	34.3	4.9	6.1

[a]Cu and K has 1 atomic % on calcined Fe/Cu/K/Al, trace amount in 10 and 20 % steam sample

TPH experiments were performed to characterize the carbonaceous species in the catalysts after different treatments. Figure 5a shows the TPH profile of Fe/Cu/K/Al after 16 h of CO reduction at 280 °C followed by 10 h of reaction at 270 °C under dry syngas flow. The profile is deconvoluted into six peaks that are assigned as (1) atomic carbon (α), (2) amorphous or polymeric carbon (β), (3) bulk iron carbides ε′-$Fe_{2.2}C$ (γ_1) and χ-$Fe_{2.5}C$ (γ_2), and (4) graphitic carbon ($\delta_1+\delta_2$) [33]. The peak temperature and carbon content are shown in Table 4.

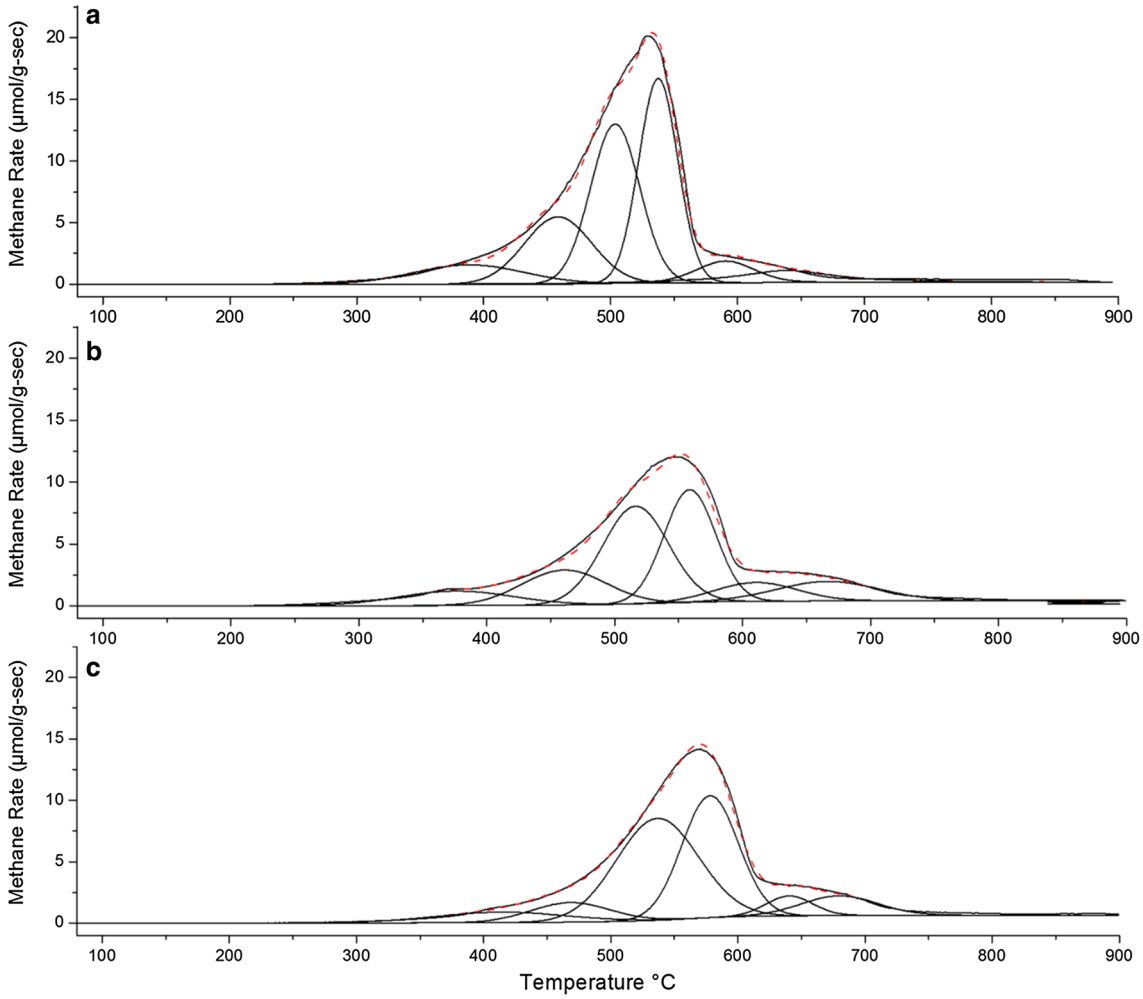

Fig. 5 TPH patterns of Fe/Cu/K/Al after pretreatment in 5 % CO/He at 280 °C for 16 h, followed by **a** treatment at 270 °C with simulated syngas (20 % CO/15 % H_2/5 % CH_4/He) for 16 h. **b** Treatment at 270 °C with simulated syngas flowed through the steam saturator for 16 h. **c** Treatment at 270 °C with simulated syngas flowed through the steam saturator for 16 h, and recarburization with 5 % CO/He at 280 °C for 16 h

Table 4 Results of TPH on Fe/Cu/K/Al after different treatments

Designation	Treatment	Peak temperature °C	Carbon content mmol/gcat	Percentage %	Type of carbon species
Dry syngas	16 h CO + 10 h syngas	388	0.23	9.6	α
		458	0.43	17.7	β
		503	0.70	28.8	γ_1
		537	0.71	29.3	γ_2
		590	0.17	6.9	δ_1
		638	0.18	7.6	δ_2
Wet syngas	16 h CO + 10 h syngas w/saturator	376	0.20	11.3	α
		460	0.26	15.3	β
		516	0.45	26.0	γ_1
		558	0.42	24.1	γ_2
		610	0.19	11.0	δ_1
		666	0.21	12.3	δ_2
Re-carburized	16 h CO + 10 h syngas w/saturator + 16 h CO	413	0.22	10.0	α
		468	0.23	10.6	β
		536	0.69	31.7	γ_1
		578	0.65	29.9	γ_2
		640	0.21	9.5	δ_1
		679	0.18	8.3	δ_2

In another test, the syngas flowed through a water saturator, carrying the moisture to simulate the reaction with steam co-feeding. As a result of steam addition, the total carbon content (1.73 mmol/gcat) on the catalyst after wet syngas treatment is lower comparing with that on the dry syngas treated catalyst (2.42 mmol/gcat). The samples with wet syngas treatment contains less iron carbides ($\gamma_1 + \gamma_2$) in both amount and percentage (Table 4). Iron carbides, especially Hägg carbides (χ-$Fe_{2.5}C$) are known to be the active phases for FTS [34–36]. Treatment with wet syngas reduced the carburization extent, which is in agreement with the loss of activity during FTS test with steam addition.

In a separate test, 5 % CO/He gas flowed through the reactor to re-carburize the catalyst after wet syngas treatment. This test is labelled as "re-carburization" and the TPH profile is shown in Fig. 5c. The total carbon content of the re-carburized catalyst is 2.18 mmol/gcat, indicating that the catalyst is only partially re-carburized after the 16 h CO treatment. The re-carburized sample contained similar amounts of α, β and δ carbon compared to the sample after wet syngas treatment in Fig. 5b, but much more carbidic carbon species ($\gamma_1 + \gamma_2$). The re-carburized sample has identical carbidic carbon content as the sample after dry syngas treatment, thus the iron carbide is recovered after the regeneration step using 5 % CO/He. The TPH results of both the wet syngas treated and the re-carburized sample show less polymeric carbon (C_β), which indicates that steam addition can remove the surface carbon [12].

The concentration of active phases for FTS (ε'-$Fe_{2.2}C$ and χ-$Fe_{2.5}C$) is lower on wet syngas treated samples. Based on the results from XRD and SEM, iron carbide was oxidized to Fe_3O_4 when steam was added in the feed, causing the catalyst deactivation during FTS. Previous studies reported that the loss of activity could be recovered once steam addition is stopped [10, 11]. For instance, Satterfield et al. [10] claim that the synthesis rate could be recovered after the removal of as much as 27 mol% steam addition. However, pure dry synthesis gas was used in their study, with H_2 and CO only. In this study, the simulated syngas contains 50 % He as inert and ~3 % of steam after passing through the saturator, yet the iron carbide is recovered after a regeneration step with 5 % CO/He. Therefore, even though the activity of Fe/Cu/K/Al catalyst was deactivated by oxidation after steam co-feeding, the iron carbide could be regenerated by flowing pure reducing gases such as CO or H_2/CO mixture.

4 Conclusion

Up to 20 % steam addition during the FTS using biomass-derived syngas has little effect on the unprompted ruthenium-based Ru/SiO_2 catalyst, except a slight decrease of conversion and methane selectivity. On the iron-based

Fe/Cu/K/Al catalyst, however, steam addition increased the WGS rate, which led to less methane selectivity and increased C_{5+} selectivity. Steam inhibited the formation of surface polymeric and carbidic carbon during the reaction. However, steam co-feeding led to the oxidation of iron carbides species especially at higher steam concentrations, thus the catalyst activity decreases drastically when steam was added to the feed. Although the iron-based catalyst could not be regenerated by the biomass-derived syngas, TPH experiments showed that the iron oxides could be partially re-carburized in more reductive carbon monoxide gas.

Acknowledgments This research is supported by U.S. Department of Agriculture, under Award Number 11-DG- 11221636-187. The help of Xiaodan Cui from Louisiana State University on Scanning electron microscopy is gratefully appreciated. We thank Kim Hutchison from North Carolina State University for the ICP-OES analysis.

References

1. Digman B, Joo HS, Kim D-S (2009) Recent progress in gasification/pyrolysis technologies for biomass conversion to energy. Environ Prog Sustain Energy 28:47–51
2. Bozell JJ, Astner A, Baker D, Biannic B, Cedeno D, Elder T, Hosseinaei O, Delbeck L, Kim J-W, O'Lenick CJ, Young T (2014) Integrating separation and conversion—conversion of biorefinery process streams to biobased chemicals and fuels. BioEnergy Res 7:856–866
3. Wang Z, Kumar N, Spivey JJ (2016) Preparation and characterization of lanthanum-promoted cobalt–copper catalysts for the conversion of syngas to higher oxygenates: formation of cobalt carbide. J Catal 339:1–8
4. Wang Z, Spivey JJ (2015) Effect of ZrO_2, Al_2O_3 and La_2O_3 on cobalt–copper catalysts for higher alcohols synthesis. Appl Catal A 507:75–81
5. Prieto G, Beijer S, Smith ML, He M, Au Y, Wang Z, Bruce DA, de Jong KP, Spivey JJ, de Jongh PE (2014) Design and synthesis of copper–cobalt catalysts for the selective conversion of synthesis gas to ethanol and higher alcohols. Angew Chem Int Ed 53:6397–6401
6. Elder T, Groom LH (2011) Pilot-scale gasification of woody biomass. Biomass Bioenergy 35:3522–3528
7. Skoulou V, Zabaniotou A, Stavropoulos G, Sakelaropoulos G (2008) Syngas production from olive tree cuttings and olive kernels in a downdraft fixed-bed gasifier. Int J Hydrogen Energy 33:1185–1194
8. Walawender WP, Chee CS, Geyer WA (1988) Influence of tree species and wood deterioration on downdraft gasifier performance. Biomass 17:51–64
9. Yates IC, Satterfield CN (1989) Effect of carbon dioxide on the kinetics of the Fischer–Tropsch synthesis on iron catalysts. Ind Eng Chem Res 28:9–12
10. Satterfield CN, Hanlon RT, Tung SE, Zou ZM, Papaefthymiou GC (1986) Effect of water on the iron-catalyzed Fischer–Tropsch synthesis. Ind Eng Chem Prod Res Dev 25:407–414
11. Pendyala VRR, Jacobs G, Mohandas JC, Luo M, Hamdeh HH, Ji Y, Ribeiro MC, Davis BH (2010) Fischer–Tropsch synthesis: effect of water over iron-based catalysts. Catal Lett 140:98–105
12. Claeys M, van Steen E (2002) On the effect of water during Fischer–Tropsch synthesis with a ruthenium catalyst. Catal Today 71:419–427
13. Dry ME (1996) Practical and theoretical aspects of the catalytic Fischer–Tropsch process. Appl Catal A 138:319–344
14. Hilmen AM, Schanke D, Hanssen KF, Holmen A (1999) Study of the effect of water on alumina supported cobalt Fischer–Tropsch catalysts. Appl Catal A 186:169–188
15. Jager B, Espinoza R (1995) Advances in low temperature Fischer–Tropsch synthesis. Catal Today 23:17–28
16. van der Laan GP, Beenackers AACM (2000) Intrinsic kinetics of the gas–solid Fischer–Tropsch and water gas shift reactions over a precipitated iron catalyst. Appl Catal A 193:39–53
17. Sharma P, Elder T, Groom LH, Spivey JJ (2013) Effect of structural promoters on Fe-based Fischer–Tropsch synthesis of biomass derived syngas. Top Catal 57:526–537
18. Mai K, Elder T, Groom LH, Spivey JJ (2015) Fe-based Fischer Tropsch synthesis of biomass-derived syngas: effect of synthesis method. Catal Commun 65:76–80
19. Jun K-W, Roh H-S, Kim K-S, Ryu J-S, Lee K-W (2004) Catalytic investigation for Fischer–Tropsch synthesis from biomass derived syngas. Appl Catal A 259:221–226
20. Dry ME (1976) Advances in Fishcher-Tropsch Chemistry. Ind Eng Chem Prod Res Dev 15:282–286
21. Botes FG (2008) The effects of water and CO_2 on the reaction kinetics in the iron-based low-temperature Fischer–Tropsch Synthesis: a literature review. Catal Rev 50:471–491
22. Ma W, Jacobs G, Graham UM, Davis BH (2013) Fischer–Tropsch synthesis: effect of K loading on the water–gas shift reaction and liquid hydrocarbon formation rate over precipitated iron catalysts. Top Catal 57:561–571
23. Storsæter S, Borg Ø, Blekkan EA, Holmen A (2005) Study of the effect of water on Fischer–Tropsch synthesis over supported cobalt catalysts. J Catal 231:405–419
24. Jacobs G, Das TK, Li J, Luo M, Patterson PM, Davis BH (2007) Fischer–Tropsch synthesis: influence of support on the impact of co-fed water for cobalt-based catalysts. In: Davis BH, Occelli ML (eds) Studies in surface science and catalysis. Elsevier, Amsterdam, pp 217–253
25. Das TK, Conner WA, Li J, Jacobs G, Dry ME, Davis BH (2005) Fischer–Tropsch synthesis: kinetics and effect of water for a Co/SiO2 catalyst. Energy Fuels 19:1430–1439
26. Das TK, Zhan X, Li J, Jacobs G, Dry ME, Davis BH (2007) Fischer–Tropsch synthesis: kinetics and effect of water for a Co/Al2O3 catalyst. In: Davis BH, Occelli ML (eds) Studies in surface science and catalysis. Elsevier, Amsterdam, pp 289–314
27. Schulz H, Claeys M, Harms S (1997) Effect of water partial pressure on steady state Fischer–Tropsch activity and selectivity of a promoted cobalt catalyst. Stud Surf Sci Catal 107:193–200
28. Yang J, Liu Y, Chang J, Wang Y-N, Bai L, Xu Y-Y, Xiang H-W, Li Y-W, Zhong B (2003) Detailed kinetics of Fischer–Tropsch synthesis on an industrial Fe–Mn catalyst. Ind Eng Chem Res 42:5066–5090
29. Lox ES, Froment GF (1993) Kinetics of the Fischer–Tropsch reaction on a precipitated promoted iron catalyst. 2. Kinetic modeling. Ind Eng Chem Res 32:71–82
30. Gnanamani MK, Jacobs G, Hamdeh HH, Shafer WD, Liu F, Hopps SD, Thomas GA, Davis BH (2016) Hydrogenation of carbon dioxide over Co–Fe bimetallic catalysts. ACS Catal 6:913–927
31. Herranz T, Rojas S, Pérez-Alonso FJ, Ojeda M, Terreros P, Fierro JLG (2006) Carbon oxide hydrogenation over silica-supported iron-based catalysts: influence of the preparation route. Appl Catal A 308:19–30

32. Lee J-F, Chern W-S, Lee M-D, Dong T-Y (1992) Hydrogenation of carbon dioxide on iron catalysts doubly promoted with manganese and potassium. Can J Chem Eng 70:511–515
33. Xu J, Bartholomew CH (2005) Temperature-programmed hydrogenation (TPH) and in situ Mössbauer spectroscopy studies of carbonaceous species on silica-supported iron Fischer–Tropsch catalysts. J Phys Chem B 109:2392–2403
34. Shultz JF, Hall WK, Seligman B, Anderson RB (1955) Studies of the Fischer–Tropsch synthesis. XIV. Hägg iron carbide as catalysts1. J Am Chem Soc 77:213–221
35. Pham TH, Qi Y, Yang J, Duan X, Qian G, Zhou X, Chen D, Yuan W (2015) Insights into Hägg iron-carbide-catalyzed Fischer–Tropsch synthesis: suppression of CH4 formation and enhancement of C–C coupling on χ-Fe_5C_2 (510). ACS Catal 5:2203–2208
36. Löchner U, Papp H, Baerns M (1986) Iron/manganese oxide catalysts for Fischer–Tropsch synthesis PART III: phase changes in iron/manganese oxide Fischer–Tropsch catalysts during start-up and synthesis process. Appl Catal 23:339–354